

See discussions, stats, and author profiles for this publication at: <https://www.researchgate.net/publication/230007482>

# Tuning the absorption spectra and nonlinear optical properties of D-π-A azobenzene derivatives by changing the dipole moment and conjugation length: A theoretical study

ARTICLE *in* JOURNAL OF PHYSICAL ORGANIC CHEMISTRY · JULY 2011

Impact Factor: 1.38 · DOI: 10.1002/poc.1792

---

CITATIONS

13

READS

21

## 3 AUTHORS, INCLUDING:



Jing Ma

Nanjing University

194 PUBLICATIONS 3,755 CITATIONS

[SEE PROFILE](#)

OCTOBER 6, 2011

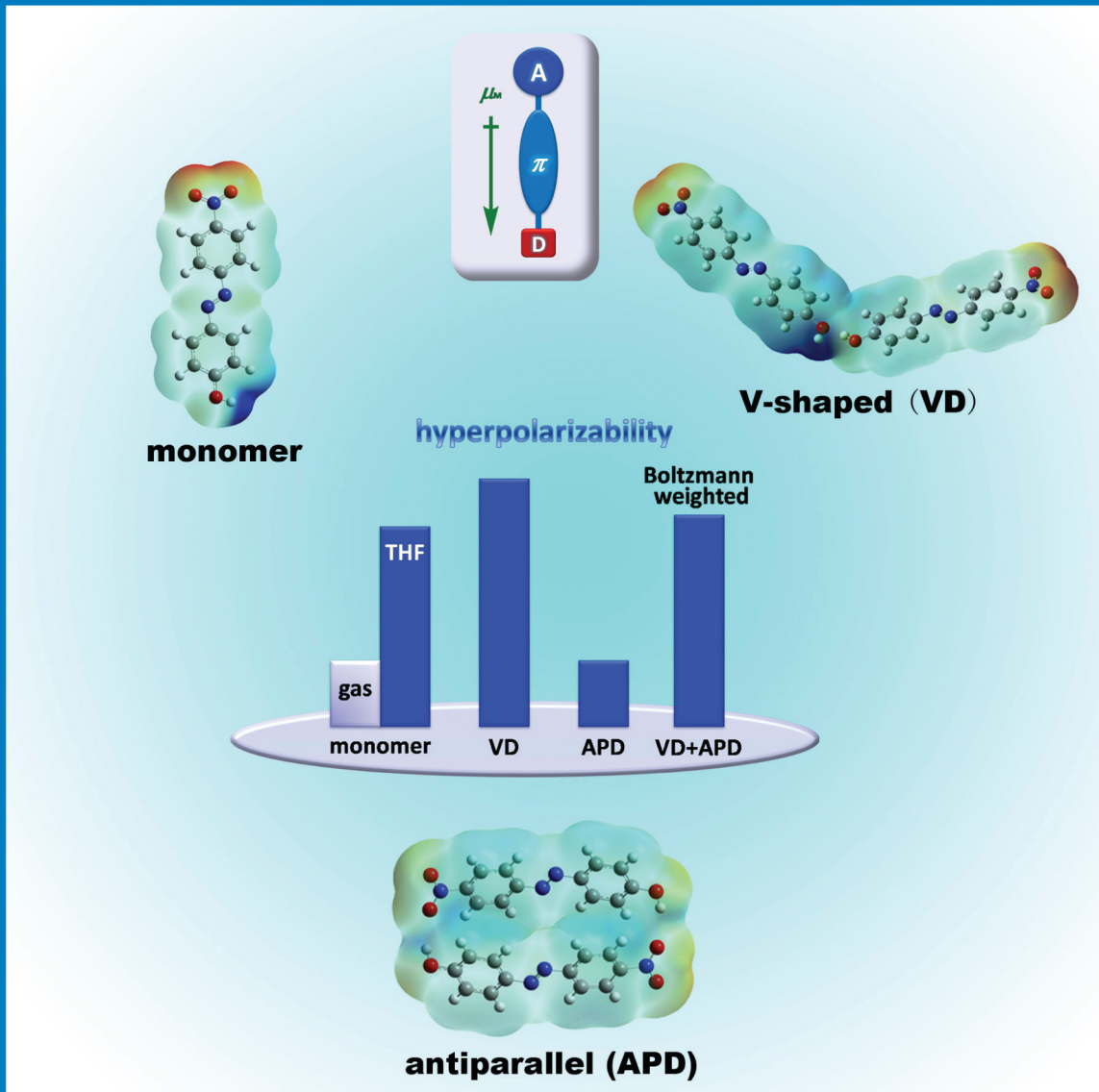
VOLUME 115

NUMBER 39

[pubs.acs.org/JPCA](http://pubs.acs.org/JPCA)

# THE JOURNAL OF PHYSICAL CHEMISTRY A

Effects of Chemical Environments and Self-Aggregations on Optical Properties Revealed through Theoretical Simulations (see page 5A)



DYNAMICS, KINETICS, ENVIRONMENTAL CHEMISTRY, SPECTROSCOPY, STRUCTURE, THEORY



ACS Publications

MOST TRUSTED. MOST CITED. MOST READ.

[www.acs.org](http://www.acs.org)

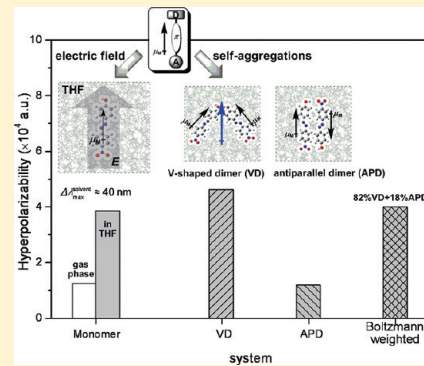
# Effects of External Electric Field and Self-Aggregations on Conformational Transition and Optical Properties of Azobenzene-Based D- $\pi$ -A Type Chromophore in THF Solution

Zeyu Liu and Jing Ma\*

Institute of Theoretical and Computational Chemistry, Key Laboratory of Mesoscopic-Chemistry of MOE, School of Chemistry and Chemical Engineering, Nanjing University, Nanjing, 210093, People's Republic of China

Supporting Information

**ABSTRACT:** The influence of environments (THF solvents and electric field) and molecular self-aggregations on the structure and optical properties of 4-(4-hydroxyphenylazo)nitrobenzene has been investigated by molecular dynamics (MD) simulations and quantum chemical calculations. Long-range electrostatic effects and the hydrogen bond interactions between the solute and the THF solvent molecules lead to the augment of nonlinear optical (NLO) response by about two times from the gas phase to THF solution, accompanied by considerable red-shift of more than 40 nm in the maximum absorption wavelengths of the ground ( $S_0$ ) and low-lying excited states ( $S_1$ ,  $S_2$ , and  $S_3$ ). The solvated chromophore reorients quickly (within 300 ps) under external electric field of 1.0 V/nm, even when the direction of the applied electric field is antiparallel to the dipole moment of the solute. Nonequilibrium MD simulations demonstrate that the light-induced *cis*–*trans* isomerization in THF solution and external electric field need longer relaxation time (about 1.0 ps) than that in gas phase (about 500 fs). The dipole–dipole interactions and intermolecular hydrogen bonds facilitate the self-aggregations of solute molecules in solution. The V-shaped dimer exhibits higher hyperpolarizability value by about 1.2 times of the monomer, whereas the antiparallel alignment leads to a cancellation of dipole moment and hence dramatic decrease in hyperpolarizability (one-third of the monomer). However, the Boltzmann-weighted contribution to hyperpolarizability from these two aggregations (with 82% V-shaped and 18% antiparallel) is close to that of the monomer. Orientations of D- $\pi$ -A dipoles in various environments and molecular aggregations are important to modulate the optical properties of materials.



## 1. INTRODUCTION

In the D- $\pi$ -A type azobenzene derivative, a strongly electron-donating (D) group and an electron-accepting (A) group are linked to a  $\pi$ -conjugated azobenzene unit. Azobenzene-based chromophores are of interest for their special electronic structures and potential applications to nonlinear optical (NLO) materials.<sup>1–10</sup> The delocalized  $\pi$ -electron distribution makes the D- $\pi$ -A systems highly polarizable. The induction of the surrounding environments, such as solvents, external electric field, and neighboring solute molecules, may result in the intramolecular charge-transfer, reorientation of dipole moments, molecular aggregates, and hence, the change in optical properties to some extent.

Though quantum chemical methods in combination with the implicit solvent models have been extensively employed to understand the environmental effects on optical properties of D- $\pi$ -A chromophores,<sup>11–13</sup> it is difficult to obtain the microscopic information of specific intermolecular interactions in complex molecular aggregates in solution. Within the Onsager solvent model and the semiempirical quantum chemical framework, the ground-state geometry was shown to be insensitive to the solvent polarity.<sup>14</sup> More sophisticated continuum dielectric models, such as polarized continuum model (PCM), worked well in describing

the optical properties of  $\pi$ -conjugated organic molecules in solvents with weak polarity.<sup>15,16</sup> However, for the highly polar solvents (such as DMSO, H<sub>2</sub>O, and CHONH<sub>2</sub>) with significant short-range intermolecular solute–solvent interactions, the combined explicit and implicit solvent models are desired.<sup>17–24</sup> The molecular mechanics (MM) is widely used to treat the explicit solvent molecules with thousands of atoms. Within the MM framework, molecular dynamics (MD) simulations have now become popular approaches to study the thermal fluctuation of solute and solvent configurations. MD simulations demonstrated that the external electric field and molecular aggregates lead to various packing configurations of the chromophores and, hence, affect the collective NLO properties. Ågren and co-workers have carried out a series of MD simulation studies on some host–guest polymeric NLO systems from which it was found that an electric field with a strength of 0.5 V/nm had a significant poling effect on the chromophore order, but little effect on the radial distribution functions of local stacking configurations in

**Received:** April 17, 2011

**Revised:** July 1, 2011

**Published:** August 10, 2011

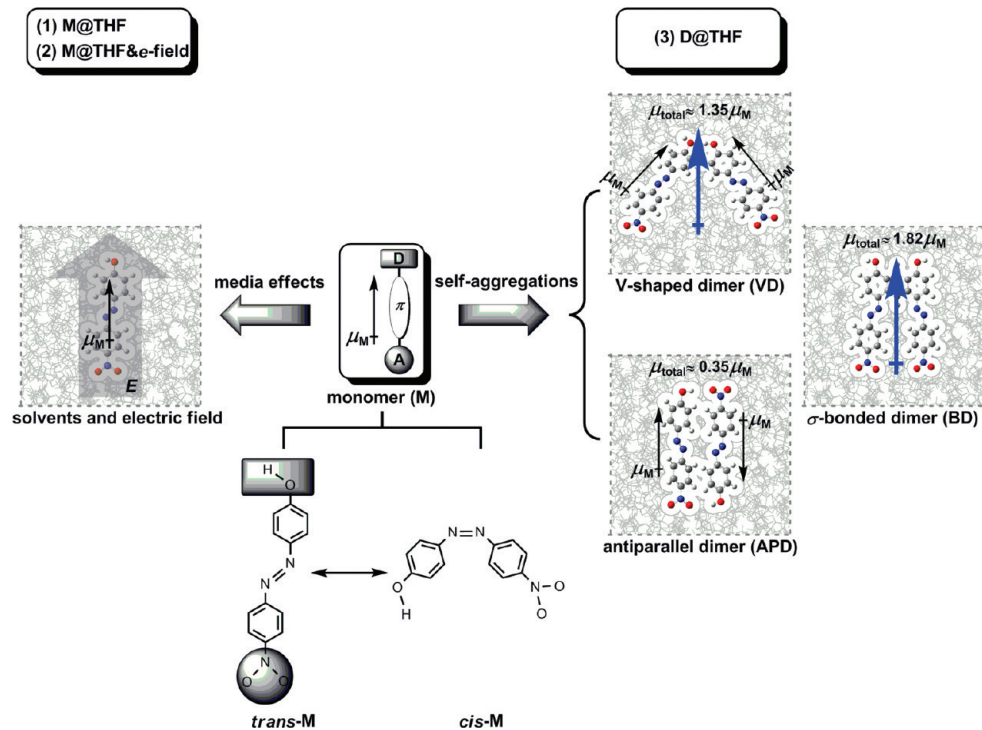


**Figure 1.** Studied models of the monomer (M) in the *trans* and the *cis* conformers, dimer (D) in V-shaped (VD), antiparallel (APD), and  $\sigma$ -bonded (BD) configurations, respectively, in THF solution.

liquid.<sup>25,26</sup> It was also shown that though the permanent dipole moment vanished for the isolated octupolar molecules, the 1,3,5-triamino-2,4,6-trinitrobenzene molecule can self-aggregate in solution due to strong intermolecular interactions.<sup>27</sup> Consequently, geometrical distortion of the molecular backbone and formation of hydrogen bonds in aggregations induced a large red-shift of the two-photon absorption spectrum.<sup>28,29</sup>

However, there is still a lack of theoretical description of the solvent effects from the widely used tetrahydrofuran (THF) solution, which has weak polarity (dielectric constant,  $\epsilon = 7.58$ ) but a strong tendency of forming a hydrogen bond with D- $\pi$ -A chromophores. Will the THF solvent molecules exert a marked influence on geometries and optical properties of the studied D- $\pi$ -A systems? Will the electric field have strong effects on the reorientations of THF solvents and solutes? It is also interesting to investigate the influence of THF solvent molecules and electric field on the *cis*-*trans* conformational transitions in solution. In the present work, we attempt to explore these fundamental questions concerning the environmental effects on configurational variations and optical properties of polarizable D- $\pi$ -A chromophore by using both the MD simulations and quantum mechanics (QM) calculations (Figure 1). It will be found that the THF solvents and electric field lead to insignificant effects on the rigid  $\pi$ -conjugated backbone, but the optical properties of both the ground and the low-lying excited states are very sensitive to the intermolecular solute–solvent interactions. We will also study two kinds of molecular aggregates, V-shaped dimer (VD) and antiparallel dimer (APD), being favored by intermolecular hydrogen bonds and the dipole–dipole interactions, respectively. Although these two kinds of arrangements have opposite effects, enhancement of the NLO properties in VD versus reduction in APD, the Boltzmann-weighted hyperpolarizability (in consideration of different contributions due to their relative thermodynamic

stability) is close to that obtained from the monomeric model. The solvated  $\sigma$ -bonded dimer (BD) in THF is also investigated for better understanding the correlation of the enhancement in the dipole moment with NLO property. The close relationship between the electrostatic polarizations (from both short-range hydrogen bond and long-range dielectric field) and the optical properties may shed insight on the future material designs and preparations.

## 2. COMPUTATIONAL DETAILS

To study the environmental (solvents and external electric field) effects on the conformational dynamics and optical properties, both MD simulations and QM calculations are employed. The computational details of MD simulations and QM calculations are presented in the following subsections.

**2.1. Validations of Force Field.** The performance of MM mainly depends on the empirical parameters of force fields. In the present work, we adopted the polymer consistent force field (PCFF),<sup>30–32</sup> which had been tested in our previous works of the packing structures of  $\pi$ -conjugated systems in amorphous phases,<sup>33,34</sup> solutions,<sup>23,24</sup> and interfaces.<sup>35–37</sup> A proper description of electrostatic interactions is crucial for describing the environmental effects on chromophores. Thus, the PCFF calculations were also performed with the natural bond orbital (NBO) and electrostatic potential (ESP) charges to survey the impact of partial atomic charges on the intermolecular interactions. The NBO and ESP charges were obtained at the level of B3LYP/6-31+G(d). To further validate the applicability of PCFF in describing the intermolecular interactions between the solute and THF molecule, the potential energy curve of O–H $\cdots$ O hydrogen bonding interaction in solute–THF dimer was tested, as depicted in Figure 2. The interaction energies were calculated at

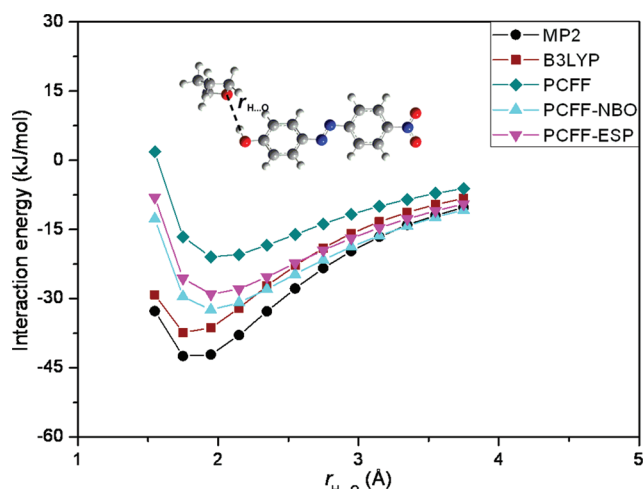


**Figure 2.** Evolutions of the interaction potential of solute and THF as a function of the intermolecular distance,  $r_{\text{H}\cdots\text{O}}$ .

MP2, B3LYP, and PCFF levels, respectively, on the basis of MP2/6-31+G(d) optimized geometry as a function of the distance between the H atom of the *trans* conformer and the O atom of THF,  $r_{\text{H}\cdots\text{O}}$ . The basis set superposition error (BSSE)<sup>38</sup> was corrected by the counterpoise method<sup>39,40</sup> for QM (MP2 and B3LYP) calculations and the interaction energies correspond to the energy difference between the complex and isolated molecules. It is demonstrated that the PCFF in combination with NBO partial charges can be used to qualitatively describe the interactions of the studied molecule in the THF solution. The adopted NBO partial charges are tabulated in Table S1.

**2.2. MD Simulations on Configurational Variations in Solution.** *MD Simulation in Canonical Ensemble.* Classical MD simulations of 4-(4-hydroxyphenylazo)nitrobenzene in explicit THF solvent molecules were performed in the canonical (NVT) ensemble with periodic boundary condition (PBC). The cubic box, in the size of  $40.76 \times 40.76 \times 40.76 \text{ \AA}^3$ , contains 500 THF molecules and the solute molecule(s). The corresponding density is about  $0.89 \text{ g/cm}^3$ . The temperature was maintained at  $T = 298 \text{ K}$  by using an Andersen thermostat<sup>41</sup> and the equation of the motion for systems was integrated using the velocity Verlet algorithm<sup>42</sup> with a time step of 1 fs. The atom-based and Ewald truncation methods were used to treat the van der Waals and Coulomb interactions, respectively, and the cutoff distances for both nonbonded interactions were set to be 15.5 Å. To study the electric field poling effect, an external electric field of 1.0 V/nm with different directions was applied after the simulation of 4800 ps.

*Nonequilibrium MD Simulation in Microcanonical Ensemble.* Among the isomers of 4-(4-hydroxyphenylazo)nitrobenzene, the *cis* isomer is less stable than the *trans* isomer by about 61.61 kJ/mol in THF solution, predicted by DFT-PCM calculations at the B3LYP/6-31+G(d) level. An illustration of the ground-state potential energy curve (solid line) of *cis*–*trans* isomerization is displayed in Figure S1. The thermal barrier of isomerization in the ground state is approximately 67.16 kJ/mol. The *trans* conformer is predominant in the ground state of this chromophore. Azobenzene derivatives can be isomerized under the irradiation of light with an appropriate wavelength. Solvents around the chromophore are expected to affect the isomerization process to some extent. The nonequilibrium MD simulations have been successfully applied

to demonstrate the photoinduced conformational dynamics of some photoswitchable peptides.<sup>43–45</sup> Here, we also employed nonequilibrium MD simulations to investigate the dynamics of *cis*–*trans* isomerization of 4-(4-hydroxyphenylazo)nitrobenzene.

In the classic force field, the ground-state potential energy cost by the torsion of N=N bond is described as follows

$$V_0 = k_0(1 - \cos 2\varphi)/2 \quad (1)$$

in which  $k_0 = 62.76 \text{ kJ/mol}$ . N=N torsional potential energy function in the ground state (dash line) obtained from eq 1 is also shown in Figure S1. To model the *cis*–*trans* photoisomerization process, Stock et al.<sup>43</sup> suggested a simple model, eq 2, to connect the excited ( $S_1$ ) *cis* state and the ground ( $S_0$ ) *trans* state.

$$V_1 = k_1(1 + \cos \varphi)/2 \quad (2)$$

Different systems require different sets of force field parameters. In this work, the parameter  $k_1$  is set to be 233.49 kJ/mol, which is derived from the vertical electronic excitation energy of the *cis* isomer in THF solution. The dotted line in Figure S1 is obtained from eq 2. It sketches the potential energy curve of photoisomerization in THF solution, going from excited *cis* conformer to the ground-state *trans* configuration.

The nonequilibrium MD simulations were carried out in the microcanonical (NVE) ensemble. The conservation energies reproduced the respective vertical electronic excitation energies of the lowest dipole-allowed excited state in gas phase and THF solution (with the details of QM calculations given in subsection 2.3). The simulations in THF solution were performed with and without the applied external electric field, respectively. Other parameters for this process are the same as those used in classical MD simulations.

All MD simulations are carried out by using the Discover module of Materials Studio package.<sup>46</sup>

**2.3. (TD)DFT Calculations on Optical Properties.** The ground and low-lying excited states of the 4-(4-hydroxyphenylazo)nitrobenzene were optimized by using the density functional theory (DFT) and time-dependent density functional theory (TDDFT),<sup>47,48</sup> respectively, with B3LYP functional and 6-31+G(d) basis set. The absorption spectra of the ground ( $S_0$ ) and low-lying excited states ( $S_1$ ,  $S_2$ , and  $S_3$ ) in THF solution ( $\epsilon = 7.58$ ) were predicted by using TDDFT calculations within the framework of the polarized continuum model (PCM).<sup>49,50</sup> The NLO properties were evaluated by using numerical differentiation of polarizabilities by the finite field (FF)<sup>51–53</sup> procedure, and the first hyperpolarizabilities reported in this work correspond to the second-harmonic generation (SHG) values.

To choose a suitable time period for sampling the electronic structure properties (dipole moments, polarizabilities and hyperpolarizabilities), we make a comparison between two different time steps, 30 ps versus 300 ps intervals, with the results shown in Table S2. The statistical result shows that the average values of dipole moments, polarizabilities, and hyperpolarizabilities with 30 ps interval during 300 ps are close to those with longer (300 ps) interval over 4500 ps. Therefore, the fluctuated geometries of the chromophore were sampled from MD snapshots at intervals of every 300 ps for achieving the compromise between the computational cost and accuracy.

All the QM calculations were performed with Gaussian 03 and Gaussian 09 programs,<sup>54,55</sup> respectively. It should be noted that different versions of the Gaussian software gave different values

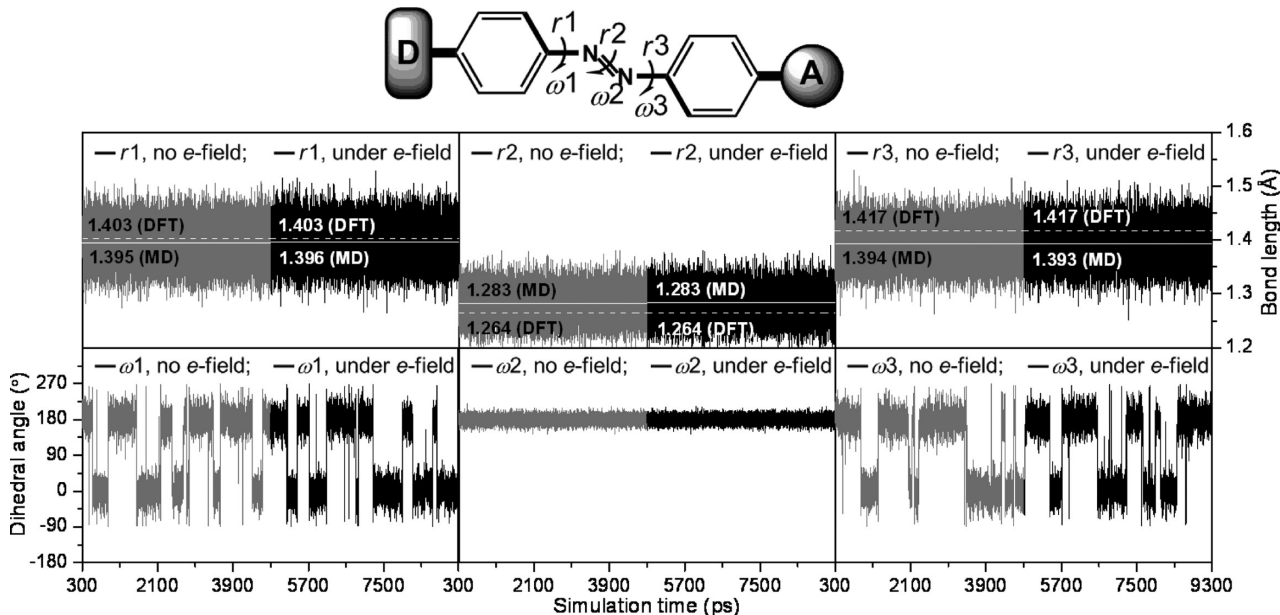


**Figure 3.** Evolutions of the selected structural parameters of the *trans* conformer. An external electric field of 1.0 V/nm is applied after 4800 ps. The average bond lengths of central C–N and N=N bonds, obtained by DFT-PCM optimizations and MD simulations, respectively, are also shown.

of response properties (cf. Figure S2) due to the different algorithms used for PCM solvation.

### 3. RESULTS AND DISCUSSION

**3.1. Media Effects from Solvents and Electric Field.** The structures and properties of D- $\pi$ -A type molecules can be tuned by various media. Here we introduce explicit THF solvents and a poling electric field to qualitatively study these effects on molecular geometry, absorption spectrum, and (hyper)polarizability.

**3.1.1. Rigid  $\pi$ -Conjugated Backbone in THF Solution.** MD simulations show the slight fluctuations in D- $\pi$ -A backbone, characterized by bond lengths of C–N ( $r_1$  and  $r_3$ ) and N=N ( $r_2$ ) as well as dihedral angles of C–C–N–N ( $\omega_1$  and  $\omega_3$ ) and C–N–N–C ( $\omega_2$ ), respectively, in THF solution. As shown in Figure 3, the average values of the selected bond lengths are 1.395 Å ( $r_1$ ), 1.283 Å ( $r_2$ ), and 1.394 Å ( $r_3$ ), respectively. Dihedral angles of  $\omega_1$  and  $\omega_3$  populated at about 0.0 and 180.0° with the equivalent weights, indicating the free rotation of rigid  $\pi$ -backbone between the electron-donating and -accepting groups. Moreover, the average value of  $\omega_2$  is about 180.1°, consistent with the planar geometry obtained from the DFT optimization.

An external electric field is applied after a 4800 ps simulation, with a strength of 1.0 V/nm along the direction parallel to the molecular dipole moment. The selected bond lengths and dihedral angles under an external poling field are also shown in Figure 3. The electric field has little impact on the geometries of the D- $\pi$ -A backbone, due to strong  $\pi$ -conjugation. To test the orientation process of the D- $\pi$ -A dipole under the external electric field, we used three kinds of electric fields with different directions, that is, parallel, crossing, and antiparallel. Figure 4a shows that the dipole moment of the chromophore reorientates quickly under the applied electric field. The reorientation process completes within a rather short time period (less than 300 ps), even when the direction of the applied electric field is antiparallel to the dipole moment (green line). Furthermore, the relative orientation between THF molecules and the solute also changed

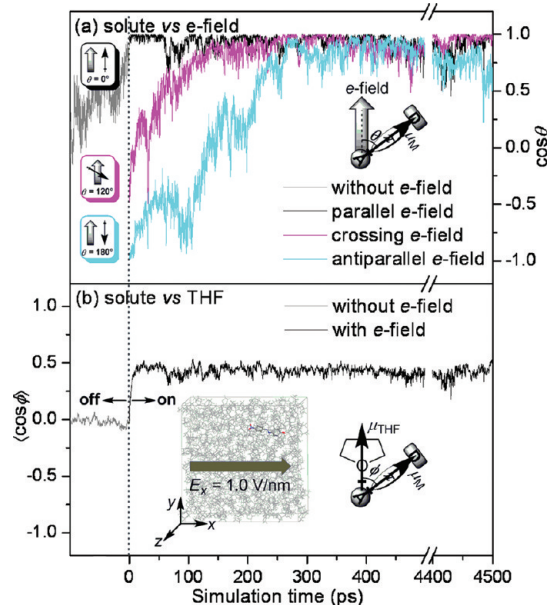


**Figure 4.** Evolutions of (a) the angle,  $\theta$ , between solute and the applied electric field and (b) the angle,  $\phi$ , between solute and THF solvents.

immediately into a partially ordered state in presence of the electric field (Figure 4b). The averaged angle between 500 THF solvents and the solute turns to be about 66° under the influence of an external poling field.

**3.1.2. Short-Range Solute–Solvent Interactions.** Though having a weak polarity, THF solvent is inclined to form hydrogen bonds with the substitute groups of the solute. Here, the O atom of THF molecule forms a strong hydrogen bond with the H atom at the donor (D) terminal of the chromophore. The local solute–solvent interactions are depicted by means of the radial distribution function (RDF),  $g(r)$ , which gives the probability of finding a solvent molecule at a distance  $r$  from the solute molecule

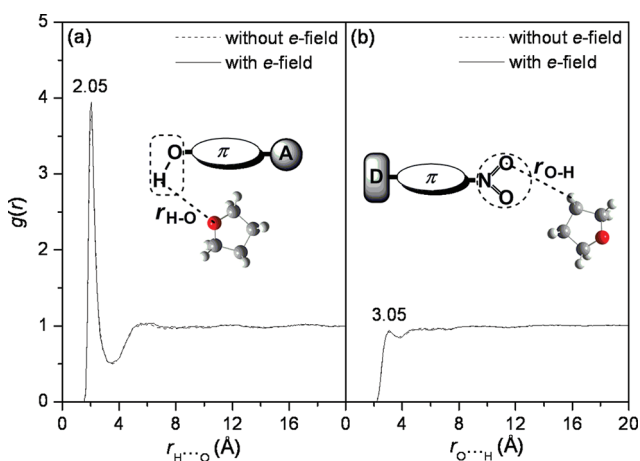


**Figure 5.** Radial distribution functions of the intermolecular  $\text{O}\cdots\text{H}$  distance,  $r_{\text{O}\cdots\text{H}}$ , at the (a) donor and (b) acceptor ends of the *trans* conformer, respectively, with or without the applied electric field in THF solution.

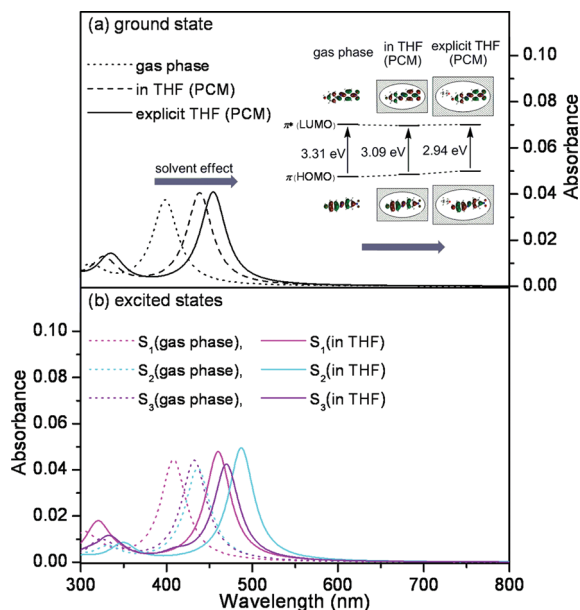
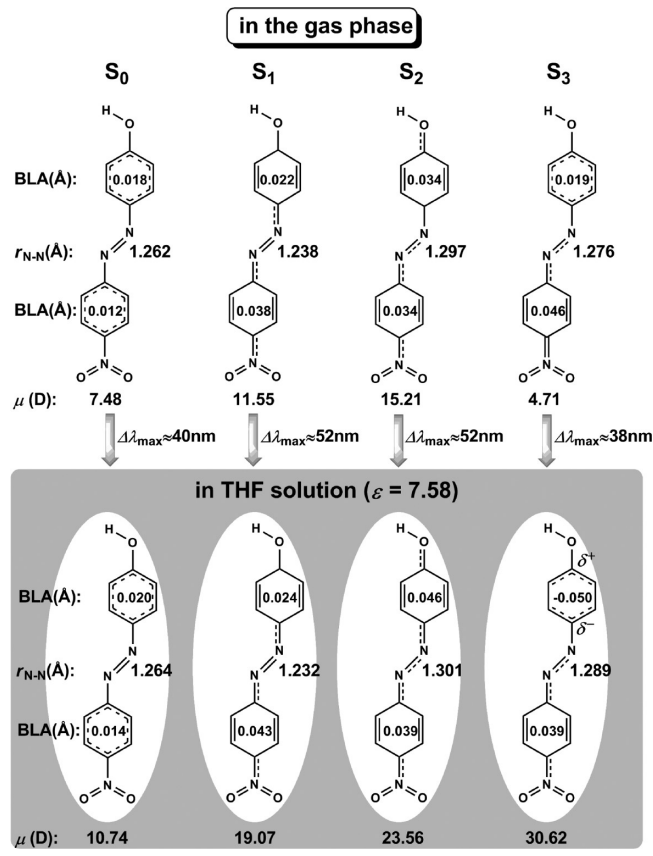


**Figure 6.** Absorption spectra of (a) ground state and (b) low-lying excited states obtained from TDDFT calculations. The Lorentzian functions are adopted with the spectral line width set to be 90 nm. The inset shows the related molecular orbitals and energy levels for the maximum adsorption.

compared to the pure solvent. The RDFs,  $g_{\text{O}-\text{H}\cdots\text{O}}(r)$  at the donor (D) end and  $g_{\text{O}\cdots\text{H}-\text{C}}(r)$  at the acceptor (A) site are presented in Figure 5. The  $r_{(\text{O})-\text{H}\cdots\text{O}}$  and  $r_{\text{O}\cdots\text{H}-(\text{C})}$  of the first solvation shell are populated at 2.05 and 3.05 Å, respectively, no matter with or without the poling field. The insignificant effect from electric field on the RDFs of the solution is consistent with the conclusions drawn from the previous MD simulations of electric field poled polymeric NLO systems.<sup>25,26</sup> As expected, the  $\text{O}-\text{H}\cdots\text{O}$  type hydrogen bond at the donor terminal is very strong because the  $r_{(\text{O})-\text{H}\cdots\text{O}}$  of about 2.05 Å is much smaller than the sum of the van der Waals radii ( $\text{H} + \text{O}$ : around 2.72 Å). The average hydrogen bonding distance also agrees with those (about 1.75–1.95 Å) obtained from QM calculations in Figure 2.

**Scheme 1.** Solvent Effects on the Ground ( $S_0$ ) and Low-Lying Excited States ( $S_1$ ,  $S_2$ , and  $S_3$ )



The significant solute–solvent hydrogen bonding interaction at the donor end will bring about a non-negligible effect on the optical properties, as addressed in the following subsection.

**3.1.3. Optical Properties.** To survey the solvent effect on absorption spectrum of the ground state ( $S_0$ ), the dipole-allowed vertical transition energies, corresponding to UV–vis absorption bands, were obtained through TDDFT calculations. We used two kinds of solvent models. The first one is the single solute molecule embedded within the framework of PCM, in which the long-range electrostatic interaction from the dielectric field is considered. The significant hydrogen bonding interaction between THF solvent and solute requires a supermolecular cluster embedded PCM model, where a solute and its nearest neighboring THF molecule are encapsulated in the cavity of the solvent reaction field. The simulated absorption spectra of the ground state are illustrated in Figure 6a. An obvious red-shift of the absorption band of the ground state is observed from the gas phase ( $\lambda_{\text{max}} = 399 \text{ nm}$ ) to THF solution ( $\lambda_{\text{max}} = 439 \text{ nm}$ ). When we considered the short-range solute–solvent interactions by introducing an explicit solvent molecule in PCM model, the lowest energy absorption band is further red-shifted to 459 nm. All these low-lying excitations are featured almost exclusively HOMO → LUMO transition, being characterized as the  $\pi\rightarrow\pi^*$  type. As shown in the inset of Figure 6a, the red-shift of the absorption band mainly stems from the promotion of the HOMO level upon the involvement of short-range solute–solvent interactions.

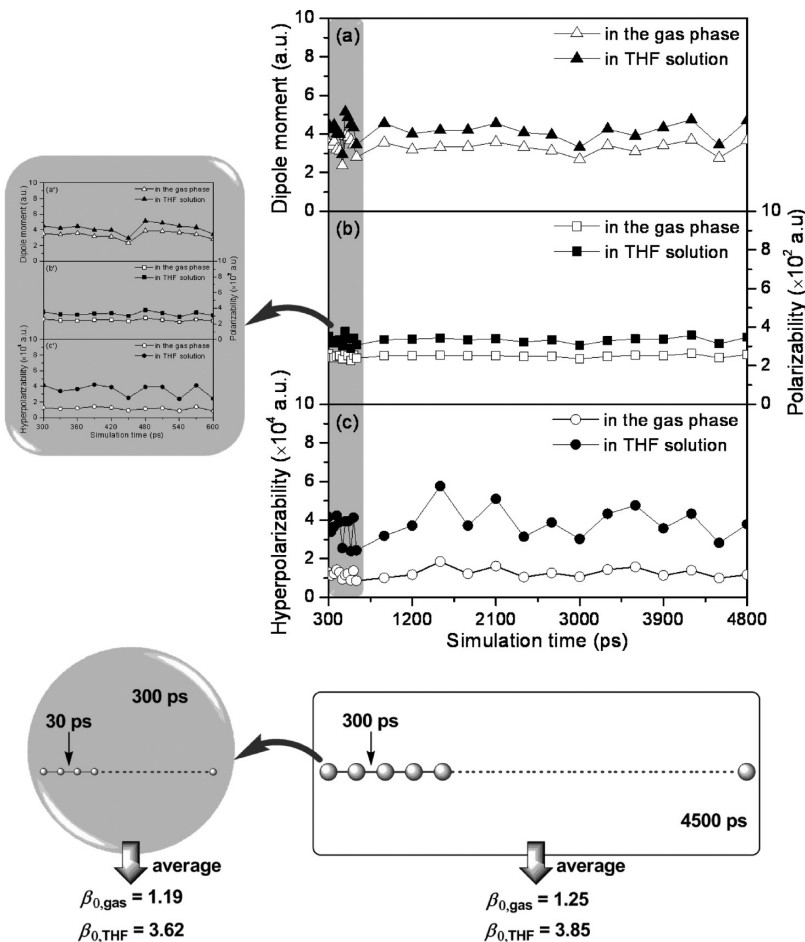


**Figure 7.** Evolutions of (a) dipole moments,  $\mu_0$ , (b) polarizabilities,  $\bar{\alpha}$ , and (c) hyperpolarizabilities,  $\beta_0$ , of the *trans* conformer without external electric field of the 300 ps interval over entire simulation. The inset shows the fluctuations in properties with a smaller time step of 30 ps interval over the period of 300 ps.

The low-lying excited states,  $S_1$ ,  $S_2$ , and  $S_3$ , have also been optimized within the framework of TDDFT-PCM using the Gaussian 09 program.<sup>55</sup> The adsorption spectra of  $S_1$ ,  $S_2$ , and  $S_3$ , calculated in the gas phase and THF solution are displayed in Figure 6b. The values of  $\lambda_{\max}$  of  $S_1$  and  $S_2$  exhibit shifts of about 52 nm to longer wavelength in the presence of the solvents. By contrast, the maximum band of  $S_3$  shows a relatively weaker redshift of about 38 nm. The difference between  $S_3$  and  $S_1$  ( $S_2$ ) is reflected from the distinct variation of the backbone and charge distribution from the gas phase to THF solution, as shown by the values of bond length alternation (BLA) and dipole moment,  $\mu$ , in Scheme 1. Here, the BLA is defined as the average difference between the C–C and C=C bond length of the phenyl ring. The increased BLA values of two phenyl rings in the chromophore imply the transition into the quinoid structure on going from the ground state ( $S_0$ ) to the lowest two excited states ( $S_1$  and  $S_2$ ). The N=N bond of the first excited state ( $S_1$ ) gains the double bond character, but  $S_2$  presents a single N–N bond character to some extent. The introduction of the dielectric field from THF solvents slightly strengthens push–pull effect with the decreased charge distribution at the donor end but increased charge distribution at the acceptor part. Hence, the THF solvents lead to a significant increase by about 1.4–1.6 times in dipole moments of the solute from the gas phase ( $S_0$ , 7.48 D;  $S_1$ , 11.55 D; and  $S_2$ , 15.21 D) to solution ( $S_0$ , 10.74 D;  $S_1$ , 19.07 D; and  $S_2$ , 23.56 D).

But the third singlet excited state,  $S_3$ , exhibits very different feature in its electronic structure. The BLAs of two phenyl rings in  $S_3$  change asymmetrically. In the gas phase, the donor-linked phenyl ring still maintains the aromatic structure with a small BLA value, but the other acceptor-linked phenyl ring shows evident quinoid electron-localization character. The N=N bond is slightly lengthened to 1.276 Å. The introduction of the long-range electrostatic effect from THF solvent molecules increased the extent of asymmetry in geometry and charge separation. In THF solution, the acceptor-linked phenyl ring takes a quinoid structure, similar to the other two excited states,  $S_1$  and  $S_2$ . But the donor-contacted phenyl ring changes into a different electronic structure with an opposite sign of BLA, that is, BLA = −0.050 Å. The N=N bond is further stretched to 1.289 Å, larger than the length in the gas phase. The dipole moment of  $S_3$  in THF solution (30.62 D) is nearly 6.5 times that (4.71 D) in the gas phase, indicating a remarkable polarization effect from the THF solvents.

The solvent effect on the molecular hyperpolarizability was also studied. The conformations were sampled from MD snapshots at intervals of every 300 ps after equilibrium. As shown in Figure 7, the fluctuations in the D- $\pi$ -A backbone have significant influence on the response properties. The average hyperpolarizability,  $\beta_0$ , in THF solution is 38539 au, which is about three times the value in the gas phase (12536 au). Moreover, solvent

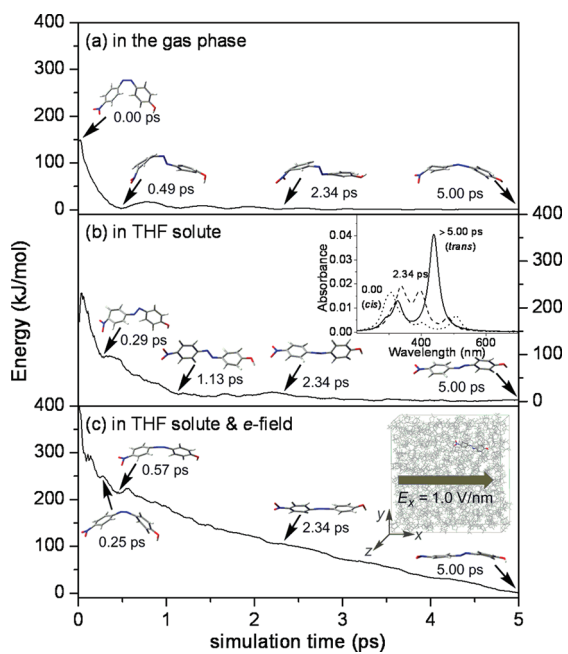


**Figure 8.** Evolutions of the potential energy along  $\text{N}=\text{N}$  *cis*–*trans* isomerization. The inset of (b) shows the time evolution of the simulated spectra along the *cis*–*trans* isomerization in THF solution. The inset of (c) shows the direction of the applied electric field.

effects are more significant on hyperpolarizability than those on the linear polarizability,  $\bar{\alpha}$ . Due to the rigid D- $\pi$ -A molecular backbone under the electric field, the poling effect on the response properties is not obvious (cf. Figure S3).

**3.1.4. *cis*–*trans* Isomerization.** Although both the ground ( $S_0$ ) and the low-lying singlet excited states ( $S_1, S_2$ , and  $S_3$ ) prefer the *trans* configuration, the central  $\text{N}=\text{N}$  bond is significantly lengthened, being accompanied with the reduced double bond character upon excitation. This permits the facile photoisomerization. Here, we are interested in the solvent effect on the photoisomerization between *cis* and *trans* isomers. The nonequilibrium MD simulations have been carried out starting from the *cis* conformer. Such a scheme has been successfully applied to study the photoisomerization dynamics of the bicyclic azobenzene peptide.<sup>43,44</sup> In this work, Figure 8 gives the time evolutions of the total potential energy along the  $\text{N}=\text{N}$  *cis*–*trans* isomerization coordinates in different environments. One can find that the isomerization, complete within 1.00 ps in every simulation for all the cases. This is similar to what was observed in azobenzene peptides, in which the *cis*–*trans* photoisomerization occurs within 250 fs after the system excited.<sup>43</sup> The steric hindrance of the solvents and intermolecular interactions result in longer relaxation time in THF solution than in the gas phase. A similar media effect has been demonstrated by QM/MM photoisomerisation simulations on 4,4'-diethoxy-azobenzene in its liquid crystalline state.<sup>56</sup> In the presence of the external electric field, the relaxation process require much longer time, due to the complexity comes from the reorientation of solute and solvents along the direction of the poling field.

The simulated spectra of the chromophore with different conformations along the *cis*–*trans* isomerization in THF solution are illustrated in the inset of Figure 8b. The calculated maximal absorption band of the *cis* isomer (at 0.00 ps) is found to be at 507 nm, featuring a main  $\pi \rightarrow \pi^*$  character. When the

simulation at 2.34 ps, two absorption peaks appear at 338 nm ( $n \rightarrow \pi^*$ ) and 396 nm ( $n \rightarrow \pi^*$ ), respectively, due to the involvement of the lone pair orbits of O atoms (of the acceptor  $-\text{NO}_2$  group) in *gauche* structure. An obvious blue-shift of  $\lambda_{\max}$  in the absorption is observed. After the system achieved equilibrium (>5.00 ps), the chromophore takes a planar *trans* conformation with the maximum absorption wavelength further red-shifted to 439 nm, corresponding to  $\pi \rightarrow \pi^*$  transition.

Several independent MD simulations were carried out to survey the local aggregation structures during the *cis*–*trans* transition. We present five typical MD trajectories in Figure 9 (without electric field) and Figure S4 (with electric field). The solvation shell of the space distribution function (SDF) within 10 Å of the  $\text{N}=\text{N}$  center obtained by the gOpenMol package<sup>57</sup> is also illustrated in Figure 9. The THF molecules evenly distribute around the center of  $\text{N}=\text{N}$  bond without specific orientational distributions. The appearance of low-energetic conformers is closely related to the short-range intermolecular contacts around the central  $\text{N}=\text{N}$  bond of solute. One can find that the closest THF molecules interact with the *cis* conformer almost in the same manner for all of these illustrations. One of the THF molecules lie in the cavity formed by a distorted molecular backbone and forms a weak hydrogen bond, with the phenyl at the end of donating group with an O (THF)···H (phenyl) distance of about 2.60–2.93 Å. Similar situations are observed under the poling electric field, as displayed in Figure S5.

**3.2. Self-Aggregation in THF Solution.** Molecular aggregate is a common phenomenon that occurs in solution, especially for those D- $\pi$ -A systems with strong dipoles. Recently, we demonstrated that there is a close relationship between the dipole moment and the NLO property of D- $\pi$ -A systems.<sup>58</sup> The orderly antiparallel alignment of the chromophore dipoles may result in the cancellation of the dipole and disappearance of the hyperpolarizability in some local configurations. There are also some possibilities of dipole enhancement by forming the nearly parallel or V-shaped alignments. Thus, we pay attention to self-aggregation effects in two typical kinds of nonbonded dimers, the V-shaped and antiparallel pairs, with the dipole enhancement and cancellation, respectively. The  $\sigma$ -bonded parallel dimer is also studied for comparison.

Plotted in Figure 10 are the angle and the distance of two moieties as a function of the MD simulation time. It is indicated that the packing structure of two parallel monomers fluctuates dramatically between the “open” and “close” states. The relative angle between long molecular axes of two moieties flips from 0.0 to 180.0° periodically. Accordingly, the intermolecular distance, defined as the distance between the geometric centers of two units, fluctuates in the range of 4.11 to 13.90 Å. This shows the competitive interplay between the dipole–dipole repulsion and the hydrogen bonding interaction at the end of each donating group. The strong electrostatic repulsion between two parallel units tends to separate them away from each other, but the hydrogen bond stabilizes this V-shaped dimer. The QM (B3LYP/6-31+G(d)-PCM) optimization adds more evidence for such competition in intermolecular interactions. The optimized V-shaped dimer is stabilized by the O···H–O hydrogen bond with an O···H distance of 2.30 Å. The binding energy, defined as  $\Delta E_b = E_D - 2E_M$ , is about  $-12.7 \text{ kJ/mol}$ . As expected, the enhancement of dipole in V-shaped stacking leads to an increase in hyperpolarizability value.

The situations are completely different for the other dimer of antiparallel orientation, as shown in Figure 10b. The favorable

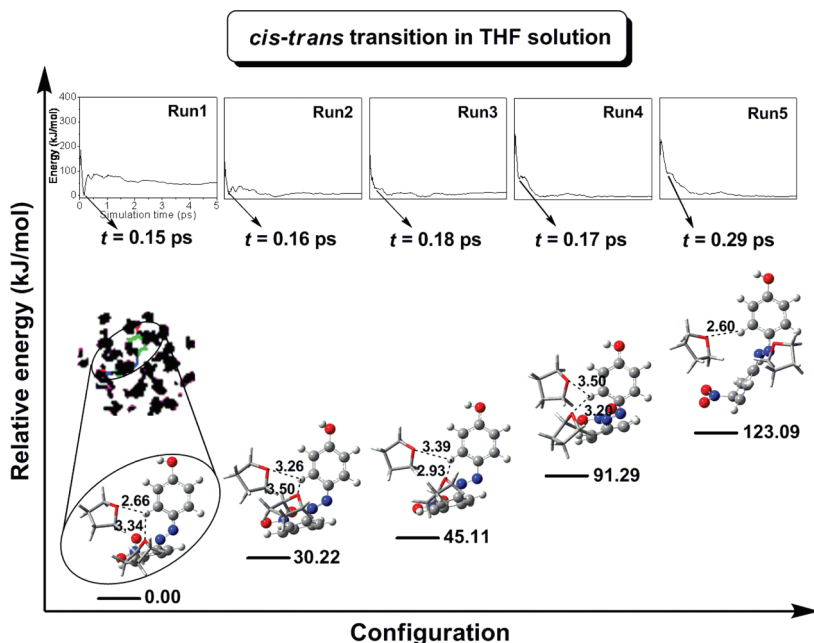


**Figure 9.** Conformers and local aggregation structures of THF solvent molecules around the  $\text{N}=\text{N}$  bond, sampled in five parallel simulations without the external electric field.

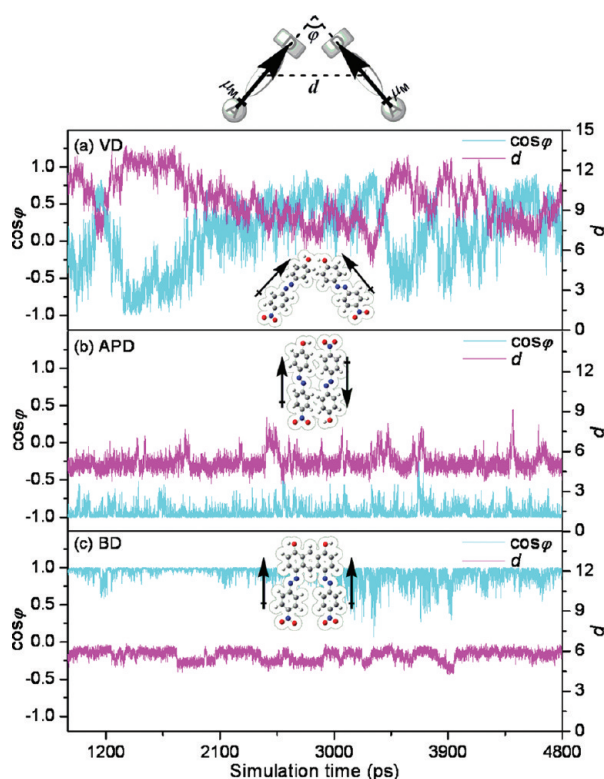


**Figure 10.** Evolutions of the angle,  $\varphi$ , and distance,  $d$ , between two units of V-shaped (VD), antiparallel (APD), and  $\sigma$ -bonded (BD) dimers.

dipole–dipole interaction and two intermolecular hydrogen bonds bind two antiparallel units tightly, and the intermolecular distance fluctuates slightly in THF solution. The binding energy of the antiparallel dimer is calculated to be  $-9.0 \text{ kJ/mol}$ , which is slightly higher than that of the V-shaped stacking. This kind of

dimer presents a small ensemble-averaged dipole moment ( $3.70 \text{ D}$ ) and hyperpolarizability ( $11911 \text{ au}$ ) due to their approximately centrosymmetric structure.

It should be mentioned that the optimized structures of the V-shaped and antiparallel dimers obtained at high level B3LYP-PCM (shown in Figure 11) are slightly different from those sampled from MD simulations, due to the ignorance of the complicated and simultaneous intermolecular interactions in the implicit solvent model.

In consideration of the difference in relative stability of these two different kinds of molecular aggregates, we obtained the Boltzmann weights of 82% for the V-shaped dimer and 18% for the antiparallel stacking, respectively. Although the V-shaped and antiparallel aggregations give opposite effects on the hyperpolarizability, the Boltzmann-weighted value (about  $40100 \text{ au}$ ) of molecular aggregates is close to that obtained from the single chromophore solvated model in THF (about  $38539 \text{ au}$ ). Apparently, the dipolar interactions and hydrogen bonds in self-aggregations destroy the ordered arrangement of the chromophores in solution and change the hyperpolarizability remarkably. Larger aggregations will also occur in the condensed phase, and further studies along this line are desired.

Different from the floppy geometry of the V-shaped dimer in THF solution, the parallel alignment of two moieties is frozen in the  $\sigma$ -bonded dimer (BD). The angle and distance between two units almost keep constant during the simulation, as shown in Figure 10c. Therefore, the dipoles of two units are nearly parallel to each other, resulting in the double in dipole moment and hyperpolarizability relative to the monomer. This implies again the orientations of D- $\pi$ -A dipoles in various environments and molecular self-aggregations are important to tune the optical properties. As addressed in previous works,<sup>1–4,9</sup> the  $\sigma$ -bonded dimer with two parallel units fixed by the nonconjugated bridge is a good candidate for the design of chromophores with high NLO response and good transparency.

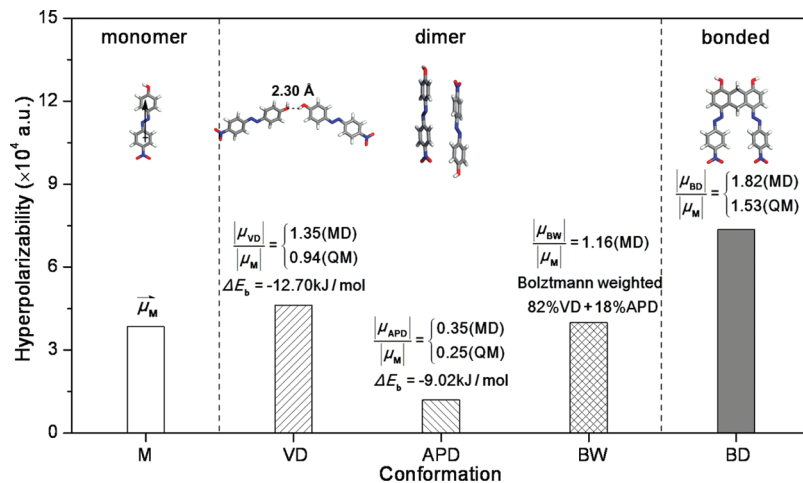


**Figure 11.** Ensemble-averaged and Boltzmann-weighted hyperpolarizabilities ( $\beta_0$ ) of monomer (M), V-shaped (VD), antiparallel (APD), and  $\sigma$ -bonded (BD) dimers, along with the ratio of dipole moments of dimers,  $\mu_{\text{VD}}$ ,  $\mu_{\text{APD}}$ , and  $\mu_{\text{BD}}$ , vs monomer ( $\mu_M$ ) and the binding energy  $\Delta E_b$  of the dimers.

## 4. CONCLUSIONS

The environmental and molecular aggregation effects on the structure and optical properties of 4-(4-hydroxyphenylazo)-nitrobenzene have been investigated by using molecular dynamics simulations and quantum chemical calculations. The D- $\pi$ -A molecular backbone is quite rigid in THF solution and the applied electric field due to the strong  $\pi$ -conjugation. However, the adsorption spectra of the ground ( $S_0$ ) and low-lying excited states ( $S_1$ ,  $S_2$ , and  $S_3$ ) and the NLO property in solution are sensitive to solvent polarity. The calculations show that the hyperpolarizability augments by about two times in THF solution relative to that in the gas phase, accompanied by a red-shift of more than 40 nm in the wavelength of the maximum absorption. The nonequilibrium MD simulations show that the *cis-trans* isomerization completes within 1.00 ps. The relaxation time is obviously longer in THF solute than that in the gas phase. The dipole–dipole interactions and intermolecular hydrogen bonds facilitate the self-aggregations of D- $\pi$ -A monomers in solution. The V-shaped aggregation dimer exhibits a 20% enhancement of hyperpolarizability relative to that of the monomer, whereas the antiparallel alignment leads to a cancellation of dipole moment and hence dramatic decrease in hyperpolarizability (one-third of the monomer). Although the V-shaped and antiparallel aggregations give opposite effects on the NLO properties, the Boltzmann-weighted hyperpolarizability (in consideration of the relative stability of these two aggregations) is close to that of the monomer. The understanding of environmental effects on structure and optical properties may be helpful to tune the performance of D- $\pi$ -A type functional materials by solvents and electric field.

## ■ ASSOCIATED CONTENT

**Supporting Information.** Force field parameters adopted in PCFF for MD simulations are tabulated in Table S1; The average values of electronic structure properties with different sampling time steps are shown in Table S2; Scheme of the  $S_0$  and  $S_1$  potential-energy curves of the monomer as a function of the  $\text{N}=\text{N}$  *cis-trans* isomerization coordinate in THF solution are displayed in Figure S1; Comparison of dipole moments ( $\mu_0$ ),

polarizabilities ( $\alpha$ ), and hyperpolarizabilities ( $\beta_0$ ) calculated by G03 and G09 are displayed in Figure S2; Evolutions of dipole moments ( $\mu_0$ ), polarizabilities ( $\alpha$ ), and hyperpolarizabilities ( $\beta_0$ ) of the *trans* conformer with external electric field are displayed in Figure S3; The conformers, along with local aggregation structures of THF solvent molecules around the  $\text{N}=\text{N}$  bond, in five parallel simulations with external electric field are displayed in Figure S4. This material is available free of charge via the Internet at <http://pubs.acs.org>.

## ■ AUTHOR INFORMATION

### Corresponding Author

\*E-mail: majing@nju.edu.cn

## ■ ACKNOWLEDGMENT

This work was supported by the National Natural Science Foundation of China (Grant No. 20825312), the Specialized Research Fund for the Doctoral Program of Higher Education of China (Grant No. 20100091110024), and the National Basic Research Program (Grant No. 2011CB808600). We are grateful to the High Performance Computing Center of Nanjing University for doing the quantum chemical calculations in this paper on its IBM Blade cluster system.

## ■ REFERENCES

- (1) Li, Z.; Li, Z.; Di, C.; Zhu, Z.; Li, Q.; Zeng, Q.; Zhang, K.; Liu, Y.; Ye, C.; Qin, J. *Macromolecules* **2006**, *39*, 6951–6961.
- (2) Li, Z.; Hu, P.; Yu, G.; Zhang, W.; Jiang, Z.; Liu, Y.; Ye, C.; Qin, J.; Li, Z. *Phys. Chem. Chem. Phys.* **2009**, *11*, 1220–1226.
- (3) Zhang, C.-Z.; Lu, C.; Zhu, J.; Lu, G.-Y.; Wang, X.; Shi, Z.-W.; Liu, F.; Cui, Y. *Chem. Mater.* **2006**, *18*, 6091–6093.
- (4) Zhang, C.-Z.; Lu, C.; Zhu, J.; Wang, C.-Y.; Lu, G.-Y.; Wang, C.-S.; Wu, D.-L.; Liu, F.; Cui, Y. *Chem. Mater.* **2008**, *20*, 4628–4641.
- (5) Smitha, P.; Asha, S. K.; Pillai, C. K. S. *J. Polym. Sci., Polym. Chem.* **2005**, *43*, 4455–4468.
- (6) Scarpaci, A.; Blart, E.; Montembault, V.; Fontaine, L.; Rodriguez, V.; Odobel, F. *ACS Appl. Mater. Interfaces* **2009**, *1*, 1799–1806.
- (7) Lanzi, M.; Paganin, L.; Cesari, G. *Macromol. Chem. Phys.* **2008**, *209*, 375–384.

- (8) Zhou, Y.; Leng, W.; Liu, X.; Xu, Q.; Feng, J.; Liu, J. *J. Polym. Sci., Polym. Chem.* **2002**, *40*, 2478–2486.
- (9) Yang, G.; Su, Z. *Int. J. Quantum Chem.* **2009**, *109*, 1553–1559.
- (10) Krawczyk, P. *J. Mol. Model.* **2010**, *16*, 659–668.
- (11) Huyskens, F. L.; Huyskens, P. L.; Persoons, A. *P. J. Chem. Phys.* **1998**, *108*, 8161–8171.
- (12) Bartkowiak, W.; Lipkowski, P. *J. Mol. Model.* **2005**, *11*, 317–322.
- (13) Bartkowiak, W.; Zaleński, R.; Niewodniczański, W.; Leszczynski, J. *J. Phys. Chem. A* **2001**, *105*, 10702–10710.
- (14) Albert, I. D. L.; Marks, T. J.; Ratner, M. *A. J. Phys. Chem.* **1996**, *100*, 9714–9725.
- (15) Tomasi, J.; Persico, M. *Chem. Rev.* **1994**, *94*, 2027–2094 and references therein.
- (16) Orozco, M.; Luque, F. *J. Chem. Rev.* **2000**, *100*, 4187–4225 and references therein.
- (17) Alemany, C.; Galembeck, S. E. *Chem. Phys.* **1998**, *232*, 151–159.
- (18) Alemany, C. *Chem. Phys. Lett.* **1999**, *302*, 461–470.
- (19) Alemany, C. *Chem. Phys.* **1999**, *244*, 151–162.
- (20) Bandyopadhyay, P.; Gordon, M. S. *J. Chem. Phys.* **2000**, *113*, 1104–1109.
- (21) Ekanayake, K. S.; Lebreton, P. R. *J. Comput. Chem.* **2006**, *27*, 277–286.
- (22) Cao, H.; Fang, T.; Li, S.; Ma, J. *Macromolecules* **2007**, *40*, 4363–4369.
- (23) Meng, S.; Ma, J.; Jiang, Y. *J. Phys. Chem. B* **2007**, *111*, 4128–4136.
- (24) Meng, S.; Ma, J. *J. Phys. Chem. B* **2008**, *112*, 4313–4322.
- (25) Tu, Y.; Zhang, Q.; Ågren, H. *J. Phys. Chem. B* **2007**, *111*, 3591–3598.
- (26) Zhang, Q.; Tu, Y.; Tian, H.; Ågren, H. *J. Phys. Chem. B* **2007**, *111*, 10645–10650.
- (27) Tu, Y.; Luo, Y.; Ågren, H. *J. Phys. Chem. B* **2005**, *109*, 16730–16735.
- (28) Liu, K.; Wang, Y.; Tu, Y.; Ågren, H.; Luo, Y. *J. Chem. Phys.* **2007**, *127*, 026101.
- (29) Liu, K.; Wang, Y.; Tu, Y.; Ågren, H.; Luo, Y. *J. Phys. Chem. B* **2008**, *112*, 4387–4392.
- (30) Hwang, M. J.; Stockfisch, T. P.; Hagler, A. T. *J. Am. Chem. Soc.* **1994**, *116*, 2515–2525.
- (31) Sun, H. *Macromolecules* **1995**, *28*, 701–712.
- (32) Sun, H.; Mumby, S. J.; Maple, J. R.; Hagler, A. T. *J. Phys. Chem.* **1995**, *99*, 5873–5882.
- (33) Zhang, G.; Pei, Y.; Ma, J.; Yin, K.; Chen, C.-L. *J. Phys. Chem. B* **2004**, *108*, 6988–6995.
- (34) Zhang, G.; Ma, J.; Wen, J. *J. Phys. Chem. B* **2007**, *111*, 11670–11679.
- (35) Pei, Y.; Ma, J. *Langmuir* **2006**, *22*, 3040–3048.
- (36) Wen, J.; Ma, J. *J. Theor. Comput. Chem.* **2009**, *8*, 677–690.
- (37) Wen, J.; Ma, J. *Langmuir* **2010**, *26*, 5595–5602.
- (38) Ransil, B. *J. J. Chem. Phys.* **1961**, *34*, 2109–2118.
- (39) Simon, S.; Duran, M.; Dannenberg, J. *J. J. Chem. Phys.* **1996**, *105*, 11024–11031.
- (40) Boys, S. F.; Bernardi, F. *Mol. Phys.* **1970**, *19*, 553–566.
- (41) Andersen, H. C. *J. Chem. Phys.* **1980**, *72*, 2384–2393.
- (42) Allen, M. P.; Tildesley, D. J. *Computational Simulation of Liquids*; Oxford: New York, 1987.
- (43) Nguyen, P. H.; Stock, G. *Chem. Phys.* **2006**, *323*, 36–44.
- (44) Nguyen, P. H.; Gorbunov, R. D.; Stock, G. *Biophys. J.* **2006**, *91*, 1224–1234.
- (45) Nguyen, P. H.; Park, S.-M.; Stock, G. *J. Chem. Phys.* **2010**, *132*, 025102.
- (46) *Materials studio*, Version 4.0; Accelrys, Inc.: San Diego, 2006.
- (47) Casida, M. K.; Jamorski, C.; Casida, K. C.; Salahub, D. R. *J. Chem. Phys.* **1998**, *108*, 4439–4449.
- (48) Stratmann, R. E.; Scuseria, G. E. *J. Chem. Phys.* **1998**, *109*, 8218–8224.
- (49) Cammi, R.; Tomasi, J. *J. Comput. Chem.* **1995**, *16*, 1449–1458.
- (50) Mennucci, B.; Tomasi, J. *J. Chem. Phys.* **1997**, *106*, 5151–5158.
- (51) Cohen, H. D.; Roothaan, C. C. J. *J. Chem. Phys.* **1965**, *43*, 534–539.
- (52) Perrin, E.; Prasad, P. N.; Mougenot, P.; Dupuis, M. *J. Chem. Phys.* **1989**, *91*, 4728–4732.
- (53) Kurtz, H. A.; Stewart, J. P.; Dieter, K. M. *J. Comput. Chem.* **1990**, *11*, 82–87.
- (54) Frisch, M. J.; Trucks, G. W.; Schlegel, H. B.; Scuseria, G. E.; Robb, M. A.; Cheeseman, J. R.; Montgomery, J. A., Jr.; Vreven, T.; Kudin, K. N.; Burant, J. C.; Millam, J. M.; Iyengar, S. S.; Tomasi, J.; Barone, V.; Mennucci, B.; Cossi, M.; Scalmani, G.; Rega, N.; Petersson, G. A.; Nakatsuji, H.; Hada, M.; Ehara, M.; Toyota, K.; Fukuda, R.; Hasegawa, J.; Ishida, M.; Nakajima, T.; Honda, Y.; Kitao, O.; Nakai, H.; Klene, M.; Li, X.; Knox, J. E.; Hratchian, H. P.; Cross, J. B.; Bakken, V.; Adamo, C.; Jaramillo, J.; Gomperts, R.; Stratmann, R. E.; Yazyev, O.; Austin, A. J.; Cammi, R.; Pomelli, C.; Ochterski, J. W.; Ayala, P. Y.; Morokuma, K.; Voth, G. A.; Salvador, P.; Dannenberg, J. J.; Zakrzewski, V. G.; Dapprich, S.; Daniels, A. D.; Strain, M. C.; Farkas, O.; Malick, D. K.; Rabuck, A. D.; Raghavachari, K.; Foresman, J. B.; Ortiz, J. V.; Cui, Q.; Baboul, A. G.; Clifford, S.; Cioslowski, J.; Stefanov, B. B.; Liu, G.; Liashenko, A.; Piskorz, P.; Komaromi, I.; Martin, R. L.; Fox, D. J.; Keith, T.; Al-Laham, M. A.; Peng, C. Y.; Nanayakkara, A.; Challacombe, M.; Gill, P. M. W.; Johnson, B.; Chen, W.; Wong, M. W.; Gonzalez, C.; Pople, J. A. *Gaussian 03*, revision D.01; Gaussian, Inc.: Wallingford, CT, 2004.
- (55) Frisch, M. J.; Trucks, G. W.; Schlegel, H. B.; Scuseria, G. E.; Robb, M. A.; Cheeseman, J. R.; Scalmani, G.; Barone, V.; Mennucci, B.; Petersson, G. A.; Nakatsuji, H.; Caricato, M.; Li, X.; Hratchian, H. P.; Izmaylov, A. F.; Bloino, J.; Zheng, G.; Sonnenberg, J. L.; Hada, M.; Ehara, M.; Toyota, K.; Fukuda, R.; Hasegawa, J.; Ishida, M.; Nakajima, T.; Honda, Y.; Kitao, O.; Nakai, H.; Vreven, T.; Montgomery, J. A.; Peralta, J. E.; Ogliaro, F.; Bearpark, M.; Heyd, J. J.; Brothers, E.; Kudin, K. N.; Staroverov, V. N.; Kobayashi, R.; Normand, J.; Raghavachari, K.; Rendell, A.; Burant, J. C.; Iyengar, S. S.; Tomasi, J.; Cossi, M.; Rega, N.; Millam, N. J.; Klene, M.; Knox, J. E.; Cross, J. B.; Bakken, V.; Adamo, C.; Jaramillo, J.; Gomperts, R.; Stratmann, R. E.; Yazyev, O.; Austin, A. J.; Cammi, R.; Pomelli, C.; Ochterski, J. W.; Martin, R. L.; Morokuma, K.; Zakrzewski, V. G.; Voth, G. A.; Salvador, P.; Dannenberg, J. J.; Dapprich, S.; Daniels, A. D.; Farkas, Ö.; Foresman, J. B.; Ortiz, J. V.; Cioslowski, J.; Fox, D. J. *Gaussian 09*, Revision A.02; Gaussian, Inc.: Wallingford, CT, 2009.
- (56) Böckmann, M.; Marx, D.; Peter, C.; Site, L. D.; Kremer, K.; Doltsinis, N. L. *Phys. Chem. Chem. Phys.* **2011**, *13*, 7604–7621.
- (57) Laaksonen, L. *J. Mol. Graphics* **1992**, *10*, 33–34.
- (58) Liu, Z.; Lu, G.-Y.; Ma, J. *J. Phys. Org. Chem.* **2011**, *24*, 568–577.